Postoperative Imaging of the Orbital Contents[1]

Michael J. Reiter, DO
Ryan B. Schwope, MD
Jonathan A. Kini, MD
Gerald E. York, MD
Abraham W. Suhr, MD

Abbreviations: GDD = glaucoma drainage device, IOP = intraocular pressure, PMMA = polymethylmethacrylate

RadioGraphics 2015; 35:221–234

Published online 10.1148/rg.351140008

Content Codes: CT HN MR NR

[1]From the Departments of Radiology (M.J.R., R.B.S., J.A.K., G.E.Y.) and Ophthalmology (A.W.S.), Brooke Army Medical Center, 3851 Roger Brooke Dr, San Antonio, TX 78234. Recipient of a Certificate of Merit award for an education exhibit at the 2013 RSNA Annual Meeting. Received March 19, 2014; revision requested June 23 and received July 2; accepted July 22. For this journal-based SA-CME activity, the authors, editor, and reviewers have disclosed no relevant relationships.)) **Address correspondence to** M.J.R. (e-mail: *mikereiter13@yahoo.com*).

SA-CME LEARNING OBJECTIVES

After completing this journal-based SA-CME activity, participants will be able to:

■ Describe the typical imaging appearances after surgery for glaucoma, cataracts, retinal detachment, globe trauma or malignancy, and facial nerve paralysis.

■ Discuss the characteristics that distinguish implanted surgical devices from orbital foreign bodies

■ List the MR imaging safety profiles of numerous implanted ophthalmologic devices.

See www.rsna.org/education/search/RG.

Ophthalmologists perform a wide array of interventions on the orbital contents. The surgical treatment of glaucoma, cataracts, retinal detachment, and ocular trauma or malignancy results in alteration of the standard anatomy, which is often readily evident at radiologic examinations. The ability to accurately recognize the various imaging manifestations after orbital surgery is critical for radiologists to avoid misdiagnosis. Of particular importance is familiarity with the numerous types of implanted devices, such as glaucoma drainage devices, orbital implants, and eyelid weights. Although knowledge of patients' surgical history is helpful, this information is often not available at the time of interpretation. Fortunately, there are characteristic posttreatment findings that enable diagnosis. The imaging features of the most commonly performed ophthalmologic procedures are highlighted, with emphasis on computed tomography and magnetic resonance (MR) imaging, because they are currently the primary modalities involved in evaluating the orbits. Glaucoma drainage devices and orbital implants after enucleation are two of the more pertinent implanted devices because their composition has substantially evolved over the past 2 decades, which affects their imaging appearance. Some devices, such as the Baerveldt Glaucoma Implant and platinum-weighted eyelid implants, may distort radiologic images. The MR imaging safety profiles of numerous implanted devices are also reported.

Introduction

Orbital imaging can be performed as a dedicated study or incidentally, since the orbits are included in the field of view when imaging the brain, face, or paranasal sinuses. Because of this, radiologists are inevitably exposed to the sequelae of numerous surgical procedures involving the globe and adnexa, several of which involve implanted devices. Awareness of the spectrum of orbital postoperative findings is imperative because their radiologic appearance can be confusing and potentially mimic pathologic entities. Knowledge of the magnetic resonance (MR) imaging safety profile of these various implanted devices is critical for imagers, as is the ability to distinguish them from foreign bodies (Table). Computed tomography (CT) and MR imaging are the two most frequently used modalities, although radiographs that encompass the orbits are occasionally encountered. In this article, the authors describe several of the more commonly performed ocular surgeries and their expected imaging features.

TEACHING POINTS

- EX-PRESS devices appear as punctate metallic areas of attenuation at CT and are typically placed superiorly or superonasally at the corneoscleral junction. Superotemporal placement is less frequent. These devices are rarely placed horizontally or inferiorly, which helps distinguish them from foreign bodies.
- Given that a fibrous encapsulated bleb is formed from aqueous humor collecting at the plate portion of GDDs, such a bleb may simulate a cystic lesion of the orbit, especially if it is large, the patient's clinical history is unknown, or the low-signal-intensity plate is not recognized. In addition to a bleb secondary to a GDD, the differential diagnosis for a cystic orbital lesion includes dermoid cyst, lymphangioma, lacrimal gland cyst, and abscess. The size of the bleb is variable, ranging from imperceptible to larger than 1 cm.
- Porous polyethylene implants are seen as hypoattenuating spherical structures at CT, with attenuation ranging from those of fat to water for the first few months after implantation. They contain internal foci of air in the early postoperative period because of their permeable central framework, which resolves over time as a result of fibrovascular ingrowth.
- Because of their high density, these implanted weights are opaque at radiography and hyperattenuating at CT, producing beam-hardening artifact. The presence of holes within a device, which are used to suture the device to the tarsus, in addition to the characteristic platelike shape and anatomic location, are diagnostic of an eyelid weight rather than a metallic foreign body.
- Finally, metallic foreign bodies can occur anywhere within the orbit. Knowledge of the patient's clinical history of prior trauma, while helpful, is not absolutely required, because the diagnosis is suggested if the object is not of a typical appearance or in a distinctive location for a surgical device or calcification.

Glaucoma

Glaucoma is the third leading cause of irreversible vision loss among adults in the United States, behind macular degeneration and diabetic retinopathy (1). It is an optic neuropathy in which injury to the optic nerve leads to characteristic peripheral vision loss. Elevated intraocular pressure (IOP) is the strongest risk factor for development of glaucoma. Lowering IOP is the only known treatment for arresting progressive optic neuropathy resulting from glaucoma. Medications represent the first line of treatment, with several surgical options available if medical management fails.

The most common glaucoma surgery is trabeculectomy, which involves creating a fistula within the superonasal, superior, or superotemporal corneoscleral junction (also known as the limbus) of the globe to drain aqueous humor from the anterior chamber into the subconjunctival space. There are no findings evident at routine postoperative CT or MR imaging after trabeculectomy.

The EX-PRESS glaucoma filtration device (Alcon, Fort Worth, Tex) was recently introduced as a way to augment the trabeculectomy procedure. This implanted device is manufactured from stainless steel and is only 2–3 mm long. It is inserted under a scleral flap and implanted at the limbus, with the proximal end under the scleral flap and the distal tip penetrating into the anterior chamber, allowing a limited outflow of aqueous humor into the intrascleral space to control IOP (Fig 1). EX-PRESS devices appear as punctate metallic areas of attenuation at CT and are typically placed superiorly or superonasally at the corneoscleral junction (Fig 2). Superotemporal placement is less frequent. These devices are rarely placed horizontally or inferiorly, which helps distinguish them from foreign bodies. At MR imaging with standard sequences, they cause susceptibility artifacts, a result of their steel construction, and appear as signal voids (Fig 3). The EX-PRESS shunt has been demonstrated to be MR imaging safe at magnet strengths up to 3 T (2).

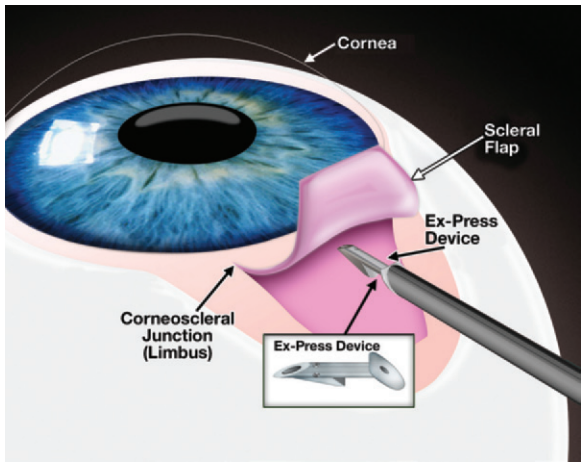

Figure 1. Illustration shows deployment of the EX-PRESS glaucoma filtration device at the limbus, highlighting its design.

Although they were initially reserved for glaucoma patients who did not respond to medical therapy or trabeculectomy, glaucoma drainage devices (GDDs) are now being used more frequently (3). GDDs consist of two parts: a tube and a plate. One end of the tube is inserted into the anterior chamber, posterior chamber, or posterior segment. The other end is attached to the plate portion of the implant, which is surgically affixed to the sclera, between the rectus muscles and under the Tenon capsule. The preferred technique is to implant GDDs within the superotemporal or inferonasal quadrants of the orbit. Implantation in the superonasal quadrant is avoided because of reported associations with Brown syndrome, also known as superior oblique tendon syndrome, because the trochlea resides there and is susceptible to injury. Brown syndrome describes the inability to elevate the adducted eye secondary to abnormality of the superior oblique tendon sheath complex (4). The surgeon's preference and the condition of patients' conjunctiva, as well as their ocular history, ultimately deter-

MR Imaging Compatibility of Implanted Devices Used by Ophthalmologists

Implanted Device	MR Imaging compatibility
EX-PRESS glaucoma filtration device	Safe up to 3 T
Glaucoma drainage devices	All types are safe
Artificial intraocular lens	All types are safe
Scleral buckles*	All types are safe
Orbital implants after enucleation	All types are safe†
Gold- and platinum-weighted eyelid implants	Safe up to 3 T
Punctal plugs	All types are safe

*Including titanium clips.
†Except older magnetic orbital implants that were used in the 1940s–1950s.

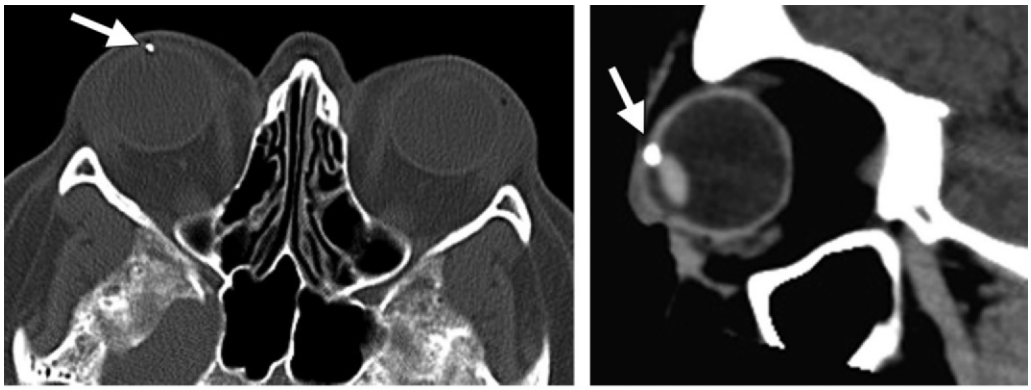

a. b.

Figure 2. Glaucoma refractory to medical management and requiring placement of an EX-PRESS device in a 48-year-old woman. Axial **(a)** and sagittal **(b)** CT images show an EX-PRESS device (arrow) in the superonasal region of the limbus of the right globe.

Figure 3. Implantation of an EX-PRESS device in a 32-year-old man with elevated IOP. Axial T2-weighted MR image shows an EX-PRESS device (arrow) in the superonasal region, which is seen as a signal void with minimal adjacent susceptibility artifact.

mines which quadrant is chosen. The purpose of the plate is to maintain a potential space between the sclera and conjunctiva. Aqueous humor flows through the tube to the plate, where it then accumulates in the potential space. The periocular vasculature of the surrounding fibrous capsule reabsorbs the aqueous humor back into the systemic circulation (5).

There are numerous types of GDDs that differ in size, material, and resistance to aqueous humor flow. The Molteno implant (Molteno Ophthalmic, Dunedin, New Zealand), Baerveldt Glaucoma Implant (Abbott Medical Optics, Santa Ana, Calif) (Fig 4), and Ahmed Glaucoma Valve (New World Medical, Rancho Cucamonga, Calif) are the three most commonly used GDDs. The Ahmed Glaucoma Valve is designed to limit flow through the tube if IOP becomes too low, a result of use of a valve with a set resistance. This characteristic prevents hypotony as a potential complication (6). The Baerveldt Glaucoma Implant and Molteno implant are both valveless.

The Baerveldt Glaucoma Implant is constructed from barium-impregnated silicone, making it the only device that is visible on radiographs (7). At CT, the plates of all three of the aforementioned GDDs are visible as a curvilinear high-attenuation structure adherent to the globe, although the Baerveldt Glaucoma Implant has even higher attenuation than the other types, with

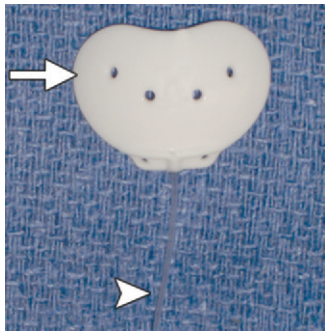

Figure 4. Photograph shows a Baerveldt Glaucoma Implant, a particular type of GDD. The Baerveldt Glaucoma Implant has a straightforward design that consists of a plate (arrow) and a tube (arrowhead). Note the holes in the plate, which are used to suture the plate to the sclera.

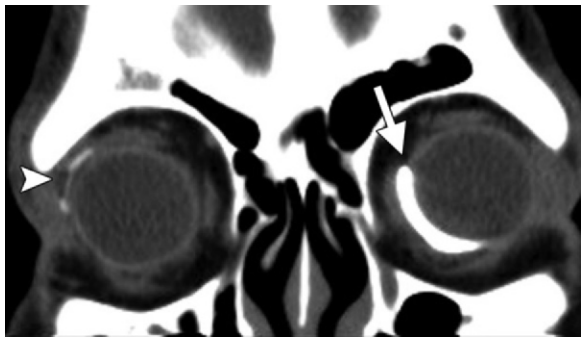

Figure 5. Bilateral GDDs with different manufacturers and designs in a 75-year-old man. Coronal CT image shows a left inferonasal Baerveldt Glaucoma Implant (arrow) and a right superotemporal Ahmed Glaucoma Valve (arrowhead). The Baerveldt Glaucoma Implant is considerably higher in attenuation because of the presence of barium. The disparate locations of the devices should not prompt concern for malposition or dislodgement of one of the devices.

a small amount of beam-hardening artifact, a result of its barium content (Fig 5). Knowledge of the imaging appearance of GDDs is important because they can be mistaken for metallic foreign bodies (8). In particular, the high attenuation of Baerveldt Glaucoma Implants makes them easily mistakable for a metallic foreign object.

Low-signal-intensity structures are seen at T1- and T2-weighted MR imaging, regardless of the type of GDD implanted. Given that a fibrous encapsulated bleb is formed from aqueous humor collecting at the plate portion of GDDs, such a bleb may simulate a cystic lesion of the orbit, especially if it is large, the patient's clinical history is unknown, or the low-signal-intensity plate is not recognized. In addition to a bleb secondary to a GDD, the differential diagnosis for a cystic orbital lesion includes dermoid cyst, lymphangioma, lacrimal gland cyst, and abscess. The size of the bleb is variable, ranging from imperceptible to larger than 1 cm (Fig 6) (6). Blebs are best depicted on T2-weighted images. Because GDDs are not ferromagnetic, they are all MR imaging safe.

Cataracts

Cataracts are the leading cause of reversible vision loss in older adults (1). The term *cataract* refers to a disease of the crystalline lens in which the lens becomes cloudy from changes in its internal protein structure, which results in decreased vision because of the critical role the lens plays in focusing light onto the retina. As many as 95% of people over the age of 65 years develop cataracts, reflecting the gradual and progressive nature of the disease (9). Although they commonly affect both eyes, they tend to develop asymmetrically. Surgery is typically indicated once vision loss becomes symptomatic.

Phacoemulsification is the most common technique for cataract removal. Ultrasonic vibrations are used to break apart the clouded lens, and an artificial intraocular lens (IOL) is implanted after removal of the native lens fragments while retaining the lens capsule. IOLs consist of two components: the optic and the footplates. The footplate components, also called haptics, exist to keep the optic in position. The overwhelming majority of IOLs are placed in the lens capsule; however, placement of the IOL in the ciliary sulcus or anterior chamber is sometimes required. Acrylic and silicone are the two most frequently used materials in IOL construction (10).

The CT and MR imaging appearances of implanted IOLs have been described and consist of a thin hyperattenuating structure and a linear structure with low T1- and T2-weighted signal intensity posterior to the iris, respectively (Fig 7) (11). These imaging characteristics reflect the properties of the optic, as the haptic portions of the IOL are not readily visible. In contrast to IOLs, the native biconvex crystalline lens is seen as an ovoid area of hyperattenuation at CT, a mildly hyperintense structure at T1-weighted MR imaging, and a hypointense structure at T2-weighted MR imaging relative to the vitreous humor. All currently used IOLs are MR imaging safe.

Retinal Detachment

The retina consists of two layers: inner and outer. The inner layer, or neurosensory retina, includes the photoreceptors. The outer layer is the retinal pigment epithelium and attaches to the inner surface of the choroid (12). The term *retinal detachment* refers to separation of the inner and outer layers. The most common mechanism of retinal detachment is tearing of the inner layer. Traction

Figure 6. MR imaging appearance of GDDs and size variability of blebs in three patients. **(a, b)** Axial T2-weighted MR images obtained in two patients show Baerveldt (arrow in **a**) and Ahmed (arrow in **b**) implants. The plate components of these GDDs are seen as thin curvilinear hypointense structures amid prominent thin-walled fluid collections, which represent blebs. Blebs can be mistaken for cystic masses if GDDs are not recognized. **(c)** Coronal T2-weighted MR image obtained in a third patient shows two right orbital Baerveldt implants. The inferonasal GDD (arrow) has a small, barely perceptible bleb associated with it, whereas the superotemporal GDD (arrowhead) has a slightly larger bleb.

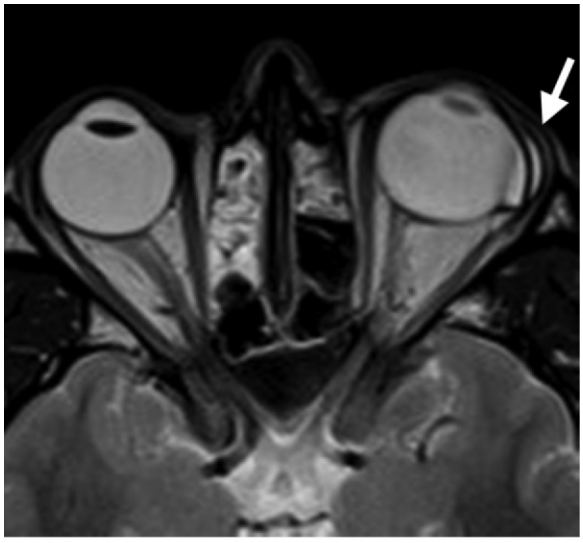

a.

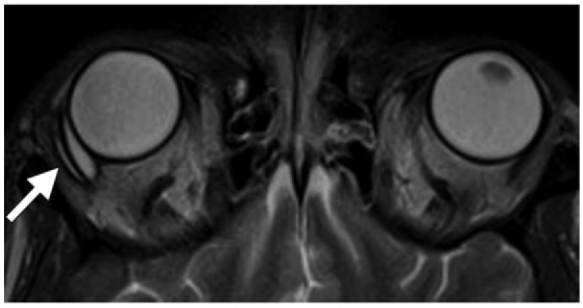

b.

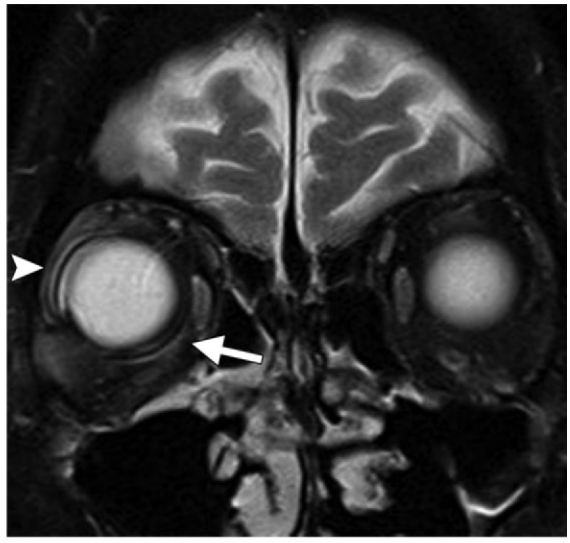

c.

or pulling on the retinal hole in conjunction with vitreous fluid entering the hole can create a potential space as the inner and outer layers separate. Retinal detachment is a surgical emergency, and treatment is necessary to prevent complications, such as retinal ischemia and blindness. The aim of surgical treatment is apposition of the two retinal layers. Several procedures are available in ophthalmologists' armamentarium to repair retinal detachments, including scleral buckling, pars plana vitrectomy with subsequent intraocular tamponade, and retinopexy. These interventions may be used simultaneously or in succession for the same eye, as needed.

Scleral buckling surgery causes an indentation of the wall of the globe, which decreases the vector forces pulling on the retina. Scleral buckles encircle the eye either in total (360°) or in a segmental fashion (less than 360° of the total globe circumference) if they are oriented perpendicular to the rectus muscles. They may also be radially oriented (parallel to the rectus muscles). Any combination of these arrangements may be applied to the eye (13). Scleral buckles are usually permanent and are removed only if complications arise. Scleral buckle devices are usually composed of silicone material, either solid silicone rubber or a porous silicone sponge. Solid silicone rubber devices are hyperattenuating at CT, whereas silicone sponge devices appear as a structure with air attenuation deforming the globe. At MR imaging, both solid silicone and silicone sponges have low signal intensity on T1- and T2-weighted images, and they can be difficult to detect (Fig 8). Indentation of the eye may be the only clue to their presence at MR imaging. Regardless of their composition, all current scleral buckle devices are MR imaging safe. In the past, tantalum clips were used to hold scleral buckle devices in place, although, currently, sutures alone are preferred. Tantalum clips are seen on radiographs and CT images as radiopaque structures, and they create susceptibility artifact at MR imaging. Tantalum is a nonferromagnetic metal and, thus, is considered MR imaging safe (14).

Vitrectomy is the process of removing the vitreous gel from the eye. Removal of the vitreous is necessary because it strongly adheres to the retina, resulting in a constant pull. Pulling on the retina allows the liquid vitreous to enter the intraretinal space in the setting of a tear of the inner retinal layer, causing separation of the two layers. At the end of the vitrectomy procedure, the eye is filled with either a long-acting gas, such as sulfur hexafluoride, or silicone oil, which serves to plug

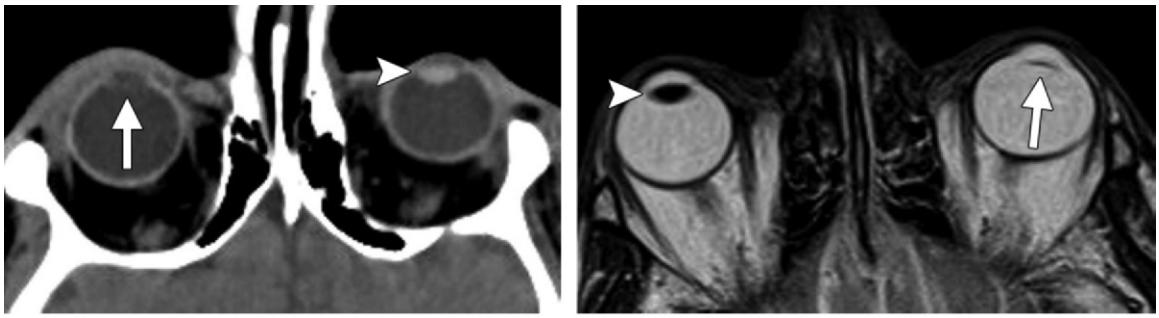

a. b.

Figure 7. Imaging appearance of artificial IOLs in two patients. **(a)** Axial CT image obtained in a 66-year-old man experiencing headaches shows an implanted IOL on the right (arrow), which is seen as a thin hyperattenuating linear structure and was incidentally found. The native biconvex crystalline lens (arrowhead) is shown on the left for comparison. **(b)** Axial T2-weighted MR image obtained in a 68-year-old man shows a left-sided IOL (arrow), which is seen as a thin hypointense linear structure in the expected region of the normal lens. The right-sided native biconvex crystalline lens (arrowhead) is shown for comparison.

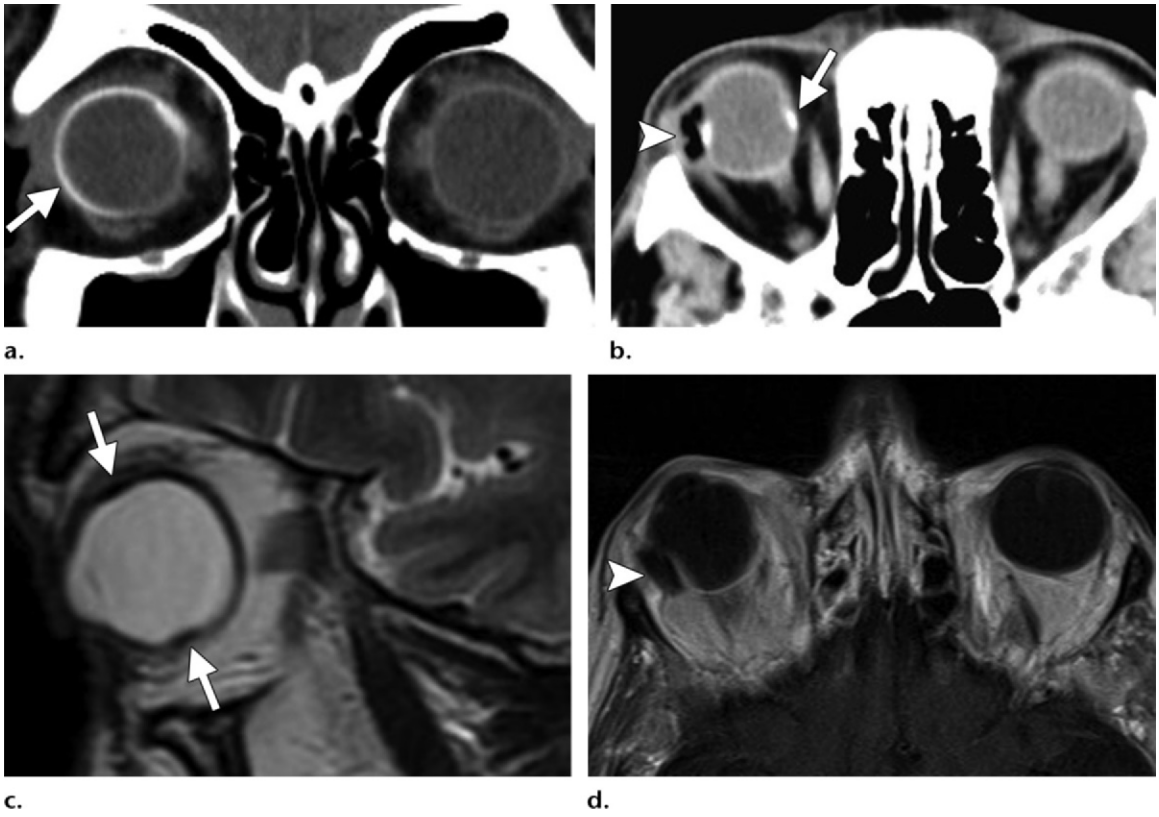

a. b. c. d.

Figure 8. Scleral buckle devices for treatment of retinal detachment in two patients. **(a)** Coronal CT image obtained in a 67-year-old man shows a a solid silicone rubber scleral buckle, which is seen as a thin hyperattenuating structure (arrow) encircling the right globe. **(b)** Axial CT image obtained in an 80-year-old woman shows a silicone sponge (arrowhead) sutured to the lateral sclera of the right globe in a radial configuration, which is seen as a structure with air attenuation. A solid circumferential silicone rubber buckle device (arrow) is also seen. **(c, d)** Sagittal T2-weighted **(c)** and axial contrast-enhanced T1-weighted **(d)** MR images obtained in the same patient as in **b** show that both the solid (arrows) and sponge (arrowhead) silicone devices have low signal intensity.

the retinal hole and prevent additional fluid from entering. However, the initial vitreous fluid that infiltrated the intraretinal space remains. One of the functions of the retinal pigment epithelium is to pump water out of the intraretinal space and into the choroid. By draining this vitreous fluid, the two retinal layers are able to reapproximate over time, relieving the retinal detachment. After intraocular gas tamponade, air attenuation is seen in the vitreous cavity at CT, with or without air-fluid levels (Fig 9). Corresponding areas of hypointensity are seen on T1- and T2-weighted MR images because of the presence of air. When silicone oil is used, it appears hyperattenuating

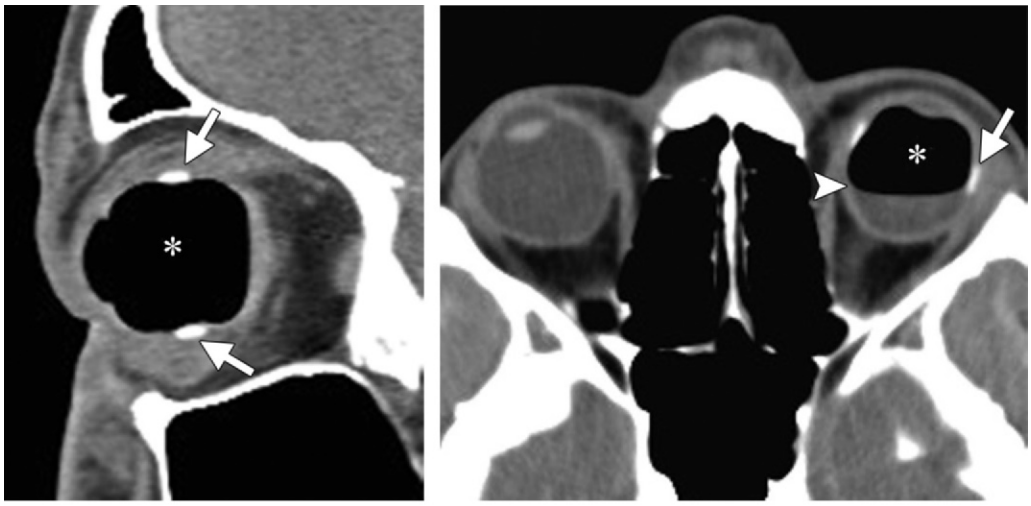

Figure 9. Vitrectomy followed by intraocular gas tamponade for treatment of retinal detachment in two patients. Sagittal CT image obtained in an 18-year-old man **(a)** and axial CT image obtained in a 34-year-old man **(b)** show an area of air attenuation within the globe (*), which represents injected sulfur hexafluoride gas. The presence of an air-fluid level (arrowhead in **b**) should not be mistaken for a postoperative infectious process. Solid silicone rubber scleral buckle devices (arrows) are also present.

at CT (15). Differentiating intraocular hemorrhage from an injection of silicone oil is possible by measuring the attenuation values (in HU). Typically, silicone is more than 100 HU, and blood is less than 90 HU, although these values may vary depending on CT scanning parameters (16). The imaging characteristics of silicone oil are somewhat variable at MR imaging because of manufacturing differences in its viscosity. Hyperintensity on T1-weighted images and iso- to hypointensity on T2-weighted images are the most commonly reported findings (17). Chemical shift artifact can be seen at the oil-water interface after injection of silicone oil (Fig 10) (18).

Retinopexy is the creation of a chorioretinal scar surrounding the retinal tear to prevent reseparation, and it can be performed with photocoagulation (laser), cryotherapy, or heat. Recently, pneumatic retinopexy has gained popularity because it can be performed in an outpatient setting. It involves the use of laser or cryotherapy retinopexy to cause adhesion between the retina and the retinal pigment epithelium surrounding the retinal breaks followed by injection of intraocular gas. Postprocedure CT or MR imaging findings of pneumatic retinopexy are similar to those of gas tamponade after vitrectomy.

Orbital Implants

For certain ocular diseases, such as phthisis bulbi, ocular malignancy, and severe trauma, enucleation may represent the only treatment option. Many different enucleation techniques exist, all of which have the common goal of removing the diseased globe intact and maintaining a cosmetically acceptable appearance (19). A spherical orbital implant is usually placed after enucleation because an anophthalmic socket will have inadequate soft-tissue volume. This results in laxity of the lower eyelid and a sunken appearance of the upper eyelid.

A variety of orbital implants are available. Silicone and polymethylmethacrylate (PMMA) were two commonly used orbital implant materials; however, they have become somewhat less popular in favor of more recently developed porous materials, such as hydroxyapatite, aluminum oxide, and porous polyethylene. These newer porous materials were devised to provide better motility and lower complication rates (20). They allow vascular ingrowth into the implant through its porous framework, which decreases the likelihood of extrusion. The extraocular muscles are attached to the orbital implant to allow physiologic movement. A removable ocular prosthesis similar to a large contact lens is then placed between the eyelids. Ocular prostheses are made from either glass or acrylic resin and are custom designed for each patient to provide an aesthetically pleasing result (21). Initially, the porous varieties of orbital implants were designed to be coupled with the ocular prosthesis with a peg device to improve motility of the prosthesis (22). However, this coupling is now rarely attempted because of the high incidence of infection and other complications that have been associated with the use of porous implants after pegging (23).

Orbital implants have a variable appearance at CT depending on their composition. Materials such as silicone and PMMA have been in use

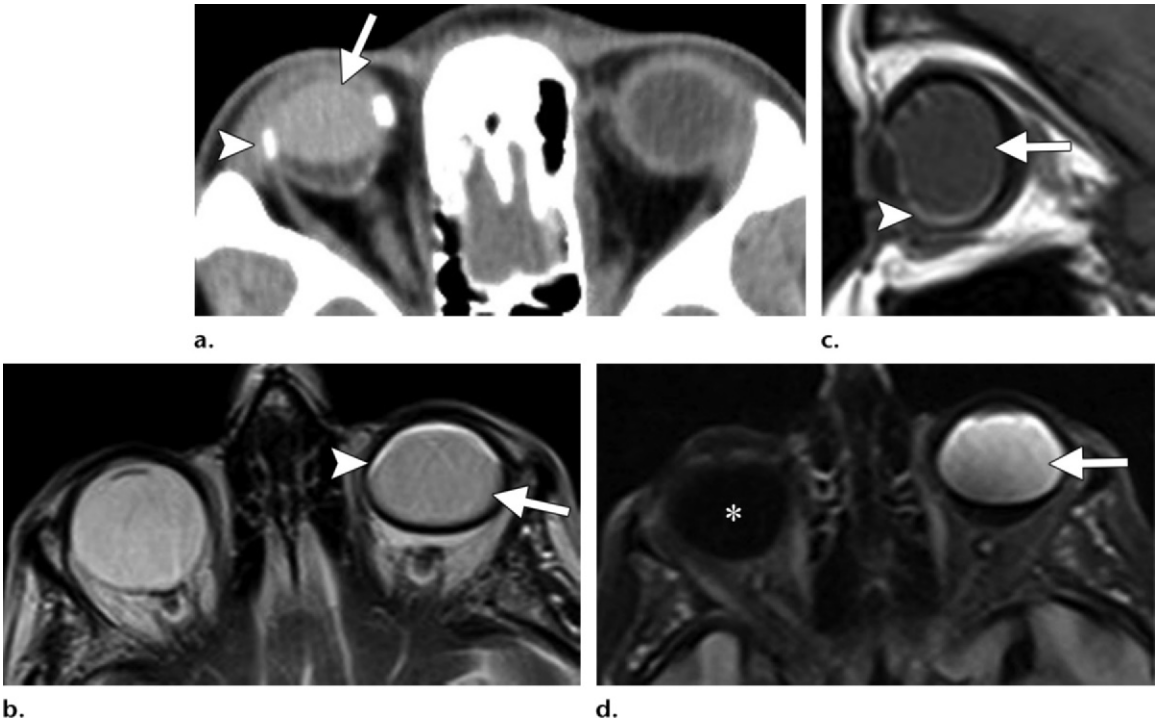

Figure 10. Vitrectomy followed by intraocular silicone oil tamponade for treatment of retinal detachment in two patients. **(a)** Axial CT image obtained in a 19-year-old man shows an area of homogeneous hyperattenuation (arrow) in the right globe, a finding that represents silicone oil. A silicone rubber buckle device (arrowhead) is also present. **(b, c)** Axial T2-weighted **(b)** and sagittal T1-weighted **(c)** MR images obtained in a 79-year-old woman show silicone oil (arrow) within the left globe. Silicone oil is mildly hypointense relative to the contralateral right vitreous humor on T2-weighted images, with corresponding intermediate signal intensity on T1-weighted images. Chemical shift artifact (arrowhead), which is seen as crescent-shaped, parallel bands of low and high signal intensity on both T1- and T2-weighted images, is seen at the oil-water interface. **(d)** Axial fluid attenuation inversion-recovery image obtained in the same patient as in **b** and **c** shows silicone oil, which is hyperintense (arrow), whereas the normal right vitreous fluid is dark (*).

for over 30 years and are radiopaque (Fig 11). Silicone implants are 440 HU, whereas, in one study, PMMA implants were 135 HU (24). Glass implants have also been used and are centrally hollow with only a thin glass rim. This construct correlates with their appearance of a high-attenuation ring with a large central area of air attenuation at CT (24).

Porous polyethylene implants are seen as hypoattenuating spherical structures at CT, with attenuation ranging from those of fat to water for the first few months after implantation (Fig 12) (25). They contain internal foci of air in the early postoperative period because of their permeable central framework, which resolves over time as a result of fibrovascular ingrowth (Fig 13). The remaining porous implant constructs—hydroxyapatite and aluminum oxide—are higher in attenuation at CT than is porous polyethylene, likely because of the presence of calcium and alumina, respectively (26). The literature about the attenuation changes of these implants over time is conflicting, specifically for hydroxyapatite, because both continued increased attenuation from bone formation and decreased attenuation from resorption of implant material associated with fibrovascular ingrowth have been reported (26,27). This may, at least in part, result from the variability of the mineral attenuation with which hydroxyapatite implants are manufactured (28). Increased fluorine-18 fluorodeoxyglucose avidity at positron emission tomography and focal radiotracer uptake at bone scintigraphy performed with technetium-99m–labeled diphosphonates have been described with porous implants and are likely secondary to physiologic fibroblast proliferation. This appearance should not be mistaken for infection or malignancy, unless there is cause for suspicion (29,30).

At MR imaging, implants made of silicone or PMMA have homogeneous dark signal intensity on T1- and T2-weighted images. Typically, porous orbital implants are mildly hyperintense on T2-weighted images, with corresponding low signal intensity on T1-weighted images (Fig 14) (31). Over time, T2-weighted signal intensity gradually decreases because of ingrowth of fibrovascular tissue. Evaluation of fibrovascular ingrowth in porous orbital implants is best performed with contrast material–enhanced MR imaging, which typically shows a centripetal pattern of enhancement (32). Currently used orbital implants are

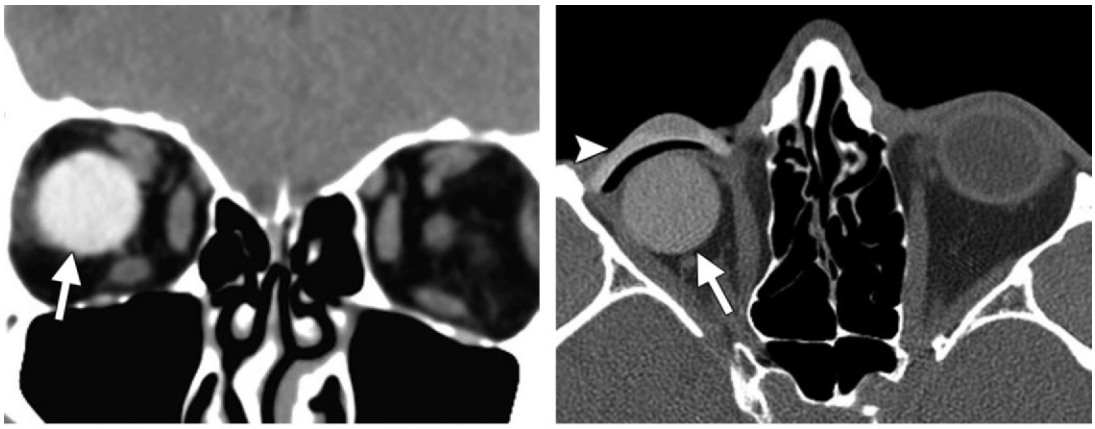

a. b.

Figure 11. CT appearance of silicone and PMMA orbital implants in two patients. **(a)** Coronal CT image obtained in a 49-year-old man with a remote history of globe rupture shows a hyperattenuating spherical implant (arrow) in the right orbit. The implant is constructed with silicone. **(b)** Axial CT image obtained in a 43-year-old man for evaluation of treatment of recent facial trauma, including an ocular injury that was treated with enucleation, shows a right-sided PMMA implant (arrow), which is homogeneously high in attenuation. Although it is dense, the PMMA implant is hypoattenuating relative to the silicone implant seen in **a**. The curvilinear area of attenuation (arrowhead) anterior to the PMMA implant represents an acrylic ocular prosthesis.

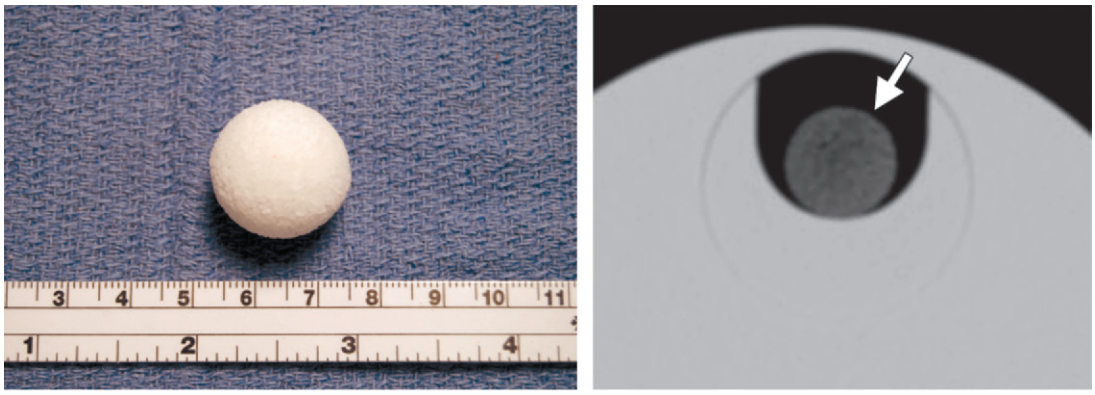

a. b.

Figure 12. Porous polyethylene orbital implant. **(a)** Photograph shows a 20-mm porous polyethylene orbital implant before insertion. **(b)** CT image obtained in a phantom with a porous polyethylene orbital implant (arrow) shows the overall low attenuation of porous polyethylene, as well as numerous internal foci of air attenuation, a result of its porous framework.

all MR imaging safe. However, caution should be taken with elderly patients in whom enucleation was performed more than 50 years ago, because a case of extrusion, presumably from MR imaging, was reported with magnetic implants used in the 1940s–1950s that are now obsolete (33).

Weighted Eyelid Implants

Paralysis of the facial nerve is a common problem and may be caused by various insults, including idiopathic, ischemic, neoplastic, and infectious causes. Incomplete eyelid closure (lagophthalmos), incomplete blinking, and abated tear production are three common complications of facial nerve paralysis that result in decreased corneal protection, which can lead to exposure keratopathy, corneal ulcers, and, potentially, corneal perforation (34). The goal of treatment is to maintain corneal lubrication, improve patient comfort, and ultimately prevent blindness. Typically, initial treatment consists of supportive care with artificial tear drops and ointments. However, patient compliance is low because of the intense regimen, and eyelid weights are an alternative therapy to avoid corneal decompensation (35).

Gold or platinum weights are implanted in the upper eyelid, just above the pupil in forward gaze, and are secured to the tarsus (a fibrous band of tissue in the eyelid) (36). Because of their high density, these implanted weights are opaque at radiography and hyperattenuating at CT, producing beam-hardening artifact (Fig 15). The presence of holes within a device, which are used to suture the device to the tarsus, in addition to

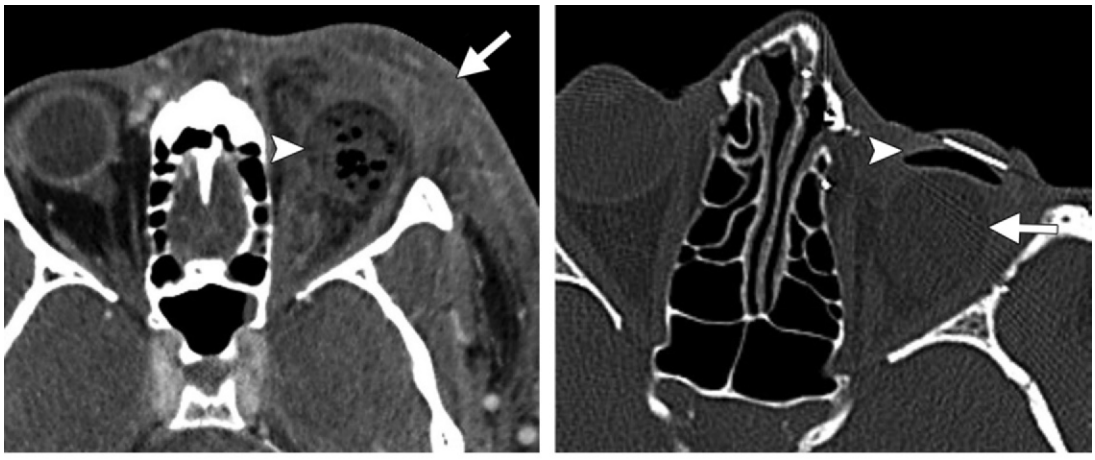

a. b.

Figure 13. Left-sided porous polyethylene orbital implant in a 40-year-old man. **(a)** Axial contrast-enhanced CT image obtained 5 days after surgery because of clinical suspicion for postoperative infection shows marked preseptal inflammatory changes (arrow) on the left, a finding consistent with cellulitis. The porous polyethylene implant (arrowhead) has internal foci of air, a result of its recent placement. However, because the radiologist presumed that an implanted device would appear radiopaque, this porous polyethylene construct was misinterpreted as a postoperative fluid collection. **(b)** Axial CT image obtained 2 months later shows resolution of the preseptal orbital cellulitis. The air within the porous polyethylene implant has also resolved secondary to fibrovascular ingrowth, and the implant now appears as a more homogeneous low-attenuation structure (arrow). Note the ocular prosthesis (arrowhead).

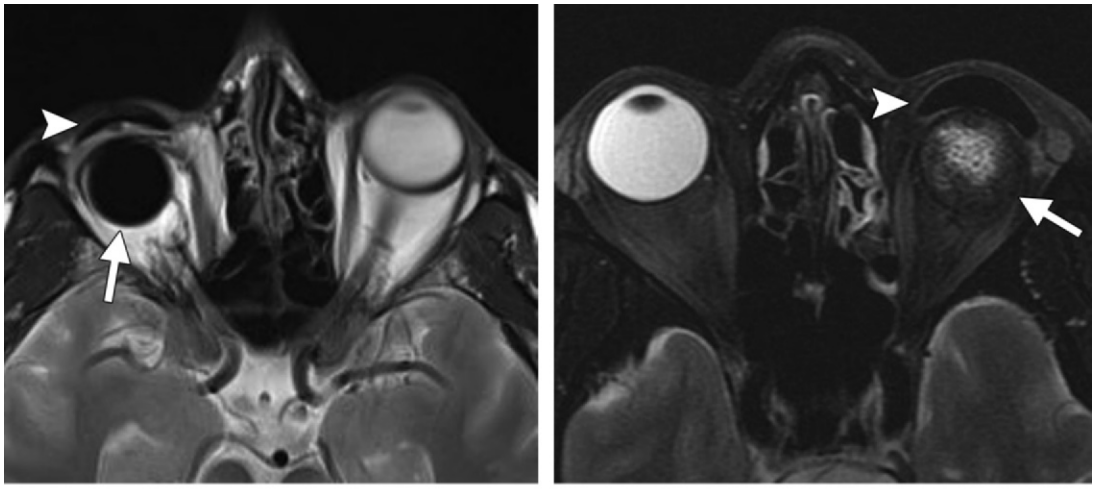

a. b.

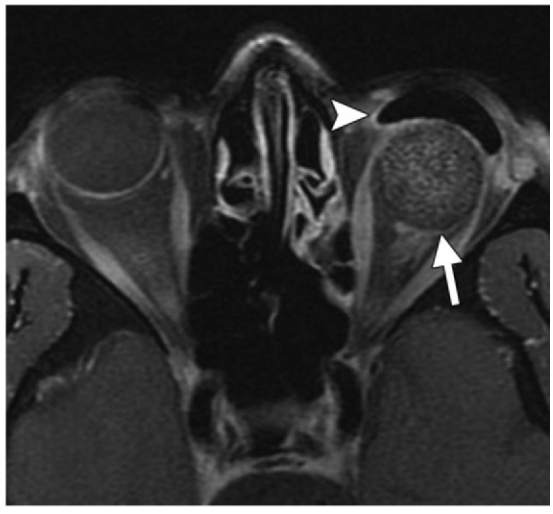

c.

Figure 14. MR imaging appearance of silicone and porous polyethylene implants in two patients. **(a)** Axial T2-weighted MR image obtained in a 49-year-old man shows a right-sided silicone orbital implant (arrow) that was placed years earlier. The implant has homogeneously low signal intensity, and there is a curvilinear focus of signal void just anterior (arrowhead), a finding that represents an ocular prosthesis. **(b)** Axial T2-weighted MR image obtained in a 42-year-old man who underwent left-sided implantation of a porous polyethylene orbital implant 8 months earlier shows the implant (arrow), which has a mild prolonged T2 relaxation time that is most pronounced centrally. **(c)** Contrast-enhanced T1-weighted fat-saturated MR image obtained in the same patient as in **b** shows enhancement of the implant (arrow), a finding indicative of fibrovascular ingrowth. An ocular prosthesis (arrowhead) is in place.

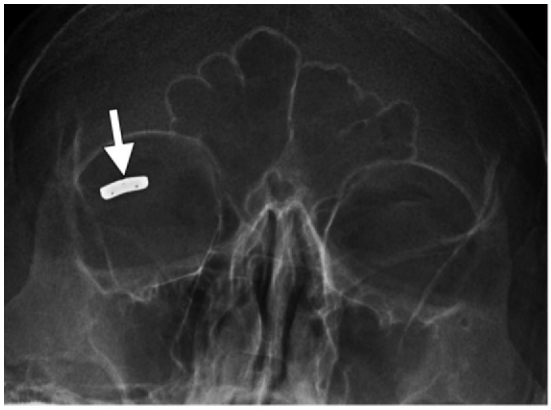

a.

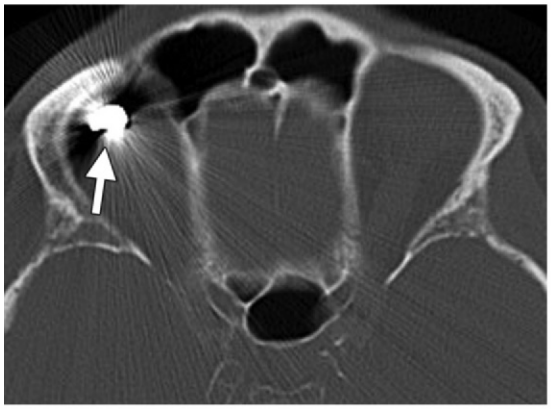

b.

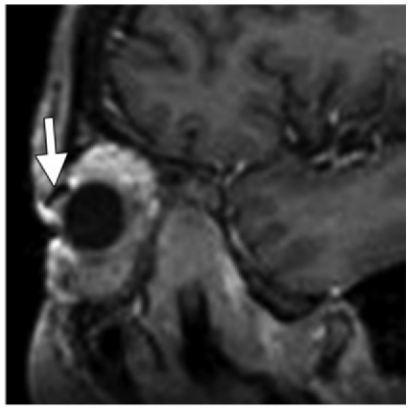

c.

Figure 15. Gold-weighted eyelid implant for corneal protection in an 80-year-old man with a history of Bell palsy. **(a, b)** Frontal radiograph **(a)** and axial CT image **(b)** show a hyperattenuating structure (arrow) in the superior right orbit. The gold weight produces a fair amount of beam-hardening artifact at CT. Holes, which are visible in the device, allow it to be sutured in place. **(c)** Sagittal contrast-enhanced T1-weighted MR image shows the gold-weighted implant (arrow) as a low-signal-intensity structure with no associated image distortion.

Figure 16. Photograph shows a silicone punctal plug (arrow) placed atop a penny for scale.

the characteristic platelike shape and anatomic location, are diagnostic of an eyelid weight rather than a metallic foreign body.

Both gold- and platinum-weighted implants appear as regions of signal void at MR imaging. Gold weights generate virtually no image distortion bcause they are not affected by the magnetic field (Fig 15), whereas platinum weights have higher paramagnetic properties and, therefore, demonstrate implant-related susceptibility artifacts (37). In vitro and animal in vivo studies have revealed both gold- and platinum-weighted implants to be MR imaging safe at currently used field strengths (38). Once an eyelid implant is identified by the radiologist at imaging, careful evaluation of the facial nerve should be undertaken (39).

Punctal Plugs

Dry eye syndrome (keratoconjunctivitis sicca) is more common in older adults and results from a myriad of factors and failures of the normal secretion of the eyes. Artificial tears and ointments are the mainstay of first-line treatment. For moderate or severe dry eye that is unresponsive to artificial tears, the use of punctal plugs can improve symptoms. Punctal plugs are inserted inside the lacrimal puncta. By blocking this outflow, tears are retained around the eye for a longer time.

Punctal plugs can be inserted in the lower eyelids, upper eyelids, or both. Permanent punctal plugs are usually made of silicone (Fig 16) (40). They are considered permanent because they do not dissolve like other collagen-based punctal plugs. However, they can dislodge without the patient's knowledge. The imaging appearance of punctal plugs has not been previously described. Because of their silicone composition, they may

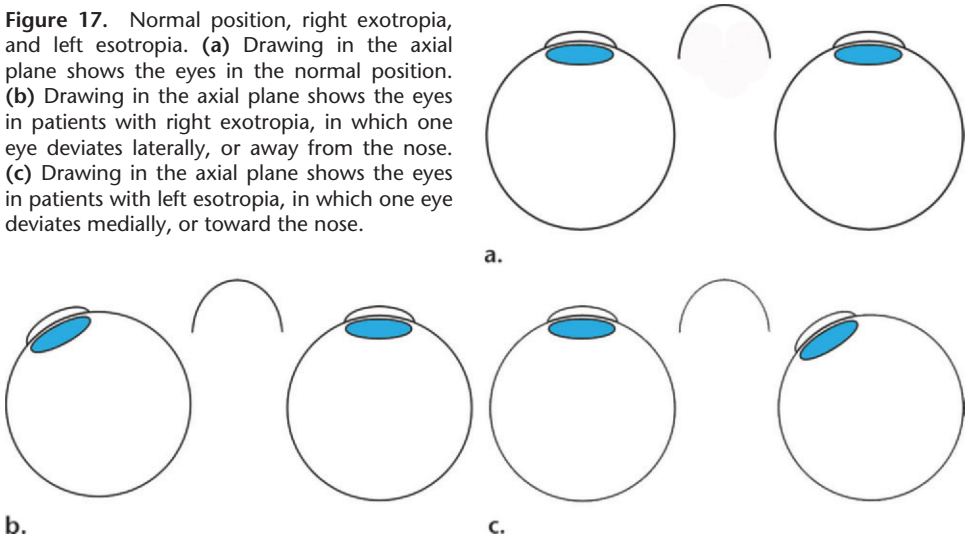

Figure 17. Normal position, right exotropia, and left esotropia. **(a)** Drawing in the axial plane shows the eyes in the normal position. **(b)** Drawing in the axial plane shows the eyes in patients with right exotropia, in which one eye deviates laterally, or away from the nose. **(c)** Drawing in the axial plane shows the eyes in patients with left esotropia, in which one eye deviates medially, or toward the nose.

appear as hyperattenuating structures at CT. However, as a result of their small size, these devices are typically not visualized at routine imaging with any modality. All currently manufactured punctal plugs are MR imaging safe.

Strabismus

Strabismus refers to any misalignment of the eyes. It is most commonly classified by the direction of eye deviation (Fig 17). Strabismus can lead to amblyopia, or decreased vision, if not detected and treated early because the brain suppresses images from the misaligned eye to prevent double vision (41). Strabismus can be divided into acquired and congenital (infantile) types. Causes of acquired strabismus include stroke, tumor, trauma, and infection (42). Although there are many surgical options for strabismus repair, recession and resection are the two most frequently performed procedures. Recession of an extraocular muscle involves detachment and relocation of the tendon on the scleral surface of the globe, usually a few millimeters posterior to its original insertion. The result is weakening of the muscle. This technique is employed for muscles contralateral to the misalignment. Resection refers to removal of a portion of the muscle, with the tendon reattached at its normal insertion site. This shortening strengthens the muscle ipsilateral to the misalignment by increasing the amount of tension produced. Changes after resection or recession of the extraocular muscles are too subtle to be evident at routine CT or MR imaging of the head and orbits.

Early results for injection of bupivacaine, an anesthetic medication, into the extraocular muscles to treat strabismus have shown promise (43). Bupivacaine selectively damages striated muscle fibers and, as a result of the repair process, causes hypertrophy and increases contractility. Enlargement of the injected muscle in comparison with the normal contralateral side is evident at MR imaging in the first few weeks to months after the procedure but eventually normalizes over time (Fig 18) (44). Awareness of this potential treatment is important so as to not misdiagnose enlargement of an extraocular muscle secondary to more insidious causes, such as neoplasm, inflammatory orbital pseudotumor, or thyroid ophthalmopathy.

Mimics of Implanted Devices

Orbital calcifications are often incidentally encountered and, unless carefully evaluated, could be mistaken for a radiopaque foreign body or an implanted device. Fortunately, these calcifications occur in characteristic locations, enabling confident diagnosis in most cases. Scleral calcifications are most common in elderly patients and are seen at the insertion sites of the medial and lateral rectus muscles; they are also referred to as senile scleral plaques (16). The trochlear apparatus is the cartilaginous structure through which the superior oblique tendon passes. Calcification in this region is observed in 25% of patients over the age of 50 years (45). Finally, metallic foreign bodies may be seen anywhere in the orbit. Knowledge of the patient's clinical history of prior trauma, while helpful, is not absolutely required to identify them; the diagnosis is suggested by an appearance and location that are not characteristic of a surgical device or calcification (Fig 19).

Conclusions

Postoperative imaging of any anatomic structure can represent a diagnostic dilemma if one is unfamiliar with the typical procedures performed. Because the orbit is frequently visualized in routine radiologic examinations, postoperative

Figure 18. Enlargement of an isolated extraocular muscle in two patients. **(a)** Axial T1-weighted MR image, obtained in a 22-year-old man with horizontal strabismus who underwent bupivacaine injection therapy to correct alignment of the eyes before treatment, shows the extraocular muscles, which have a symmetric appearance, specifically the left lateral rectus (arrow). **(b)** Axial T1-weighted MR image obtained 6 weeks after injection of bupivacaine shows mild diffuse enlargement of the left lateral rectus muscle (arrow) compared with the pretreatment image. **(c)** Axial T1-weighted MR image obtained in a 39-year-old woman with right orbital pain and proptosis shows enlargement of only the right lateral rectus muscle (arrow). The clinical and radiologic findings suggested orbital pseudotumor, and symptoms completely resolved after corticosteroid therapy. Knowledge of the clinical scenario is critical, because these imaging findings are almost identical to those seen in **b**.

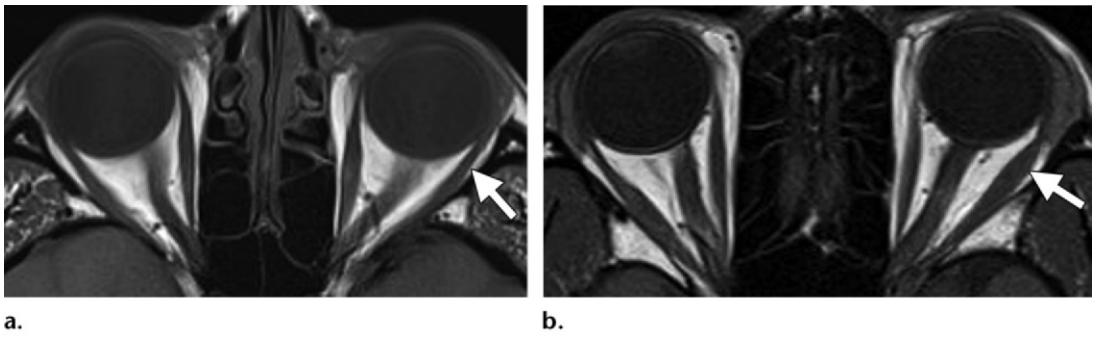

a. **b.**

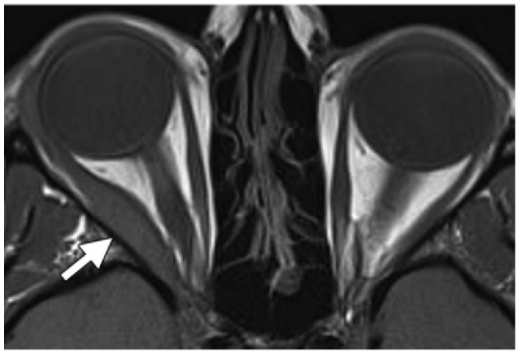

c.

changes of the globe and adnexa are invariably encountered. The radiologist's knowledge of expected imaging findings after orbital interventions can prevent confusion and misdiagnosis of implanted devices.

References

1. Congdon N, O'Colmain B, Klaver CC, et al. Causes and prevalence of visual impairment among adults in the United States. Arch Ophthalmol 2004;122(4):477–485.
2. Geffen N, Trope GE, Alasbali T, Salonen D, Crowley AP, Buys YM. Is the Ex-PRESS glaucoma shunt magnetic resonance imaging safe? J Glaucoma 2010;19(2):116–118.
3. Hong CH, Arosemena A, Zurakowski D, Ayyala RS. Glaucoma drainage devices: a systematic literature review and current controversies. Surv Ophthalmol 2005;50(1):48–60.
4. Ball SF, Ellis GS Jr, Herrington RG, Liang K. Brown's superior oblique tendon syndrome after Baerveldt glaucoma implant. Arch Ophthalmol 1992;110(10):1368.
5. Reiter M, Schwope R, Walker K, Suhr A. Imaging of glaucoma drainage devices. J Comput Assist Tomogr 2012;36(2):277–279.
6. Jeon TY, Kim HJ, Kim ST, Chung TY, Kee C. MR imaging features of giant reservoir formation in the orbit: an unusual complication of Ahmed glaucoma valve implantation. AJNR Am J Neuroradiol 2007;28(8):1565–1566.
7. Schwartz KS, Lee RK, Gedde SJ. Glaucoma drainage implants: a critical comparison of types. Curr Opin Ophthalmol 2006;17(2):181–189.
8. Ceballos EM, Parrish RK 2nd. Plain film imaging of Baerveldt glaucoma drainage implants. AJNR Am J Neuroradiol 2002;23(6):935–937.
9. Sharkness CM, Hamburger S, Kaczmarek RG, Hamilton PM, Bright RA, Moore RM Jr. Racial differences in the prevalence of intraocular lens implants in the United States. Am J Ophthalmol 1992;114(6):667–674.
10. Kuo MD, Hayman LA, Lee AG, Mayo GL, Diaz-Marchan PJ. In vivo CT and MR appearance of prosthetic intraocular lens. AJNR Am J Neuroradiol 1998;19(4):749–753.
11. Aksoy FG, Gomori JM, Halpert M. CT and MR imaging of contact lenses and intraocular lens implants. Comput Med Imaging Graph 1999;23(4):205–208.
12. Mafee MF, Karimi A, Shah J, Rapoport M, Ansari SA. Anatomy and pathology of the eye: role of MR imaging and CT. Neuroimaging Clin N Am 2005;15(1):23–47.
13. Lane JI, Watson RE Jr, Witte RJ, McCannel CA. Retinal detachment: imaging of surgical treatments and complications. RadioGraphics 2003;23(4):983–994.
14. Bakshandeh H, Shellock FG, Schatz CJ, Morisoli SM. Metallic clips used for scleral buckling: ex vivo evaluation of ferromagnetism at 1.5 T. J Magn Reson Imaging 1993;3(3):559.
15. Mathews VP, Elster AD, Barker PB, Buff BL, Haller JA, Greven CM. Intraocular silicone oil: in vitro and in vivo MR and CT characteristics. AJNR Am J Neuroradiol 1994;15(2):343–347.
16. LeBedis CA, Sakai O. Nontraumatic orbital conditions: diagnosis with CT and MR imaging in the emergent setting. RadioGraphics 2008;28(6):1741–1753.
17. Herrick RC, Hayman LA, Maturi RK, Diaz-Marchan PJ, Tang RA, Lambert HM. Optimal imaging protocol after intraocular silicone oil tamponade. AJNR Am J Neuroradiol 1998;19(1):101–108.
18. Herrick RC, Hayman LA, Taber KH, Diaz-Marchan PJ, Kuo MD. Artifacts and pitfalls in MR imaging of the orbit: a clinical review. RadioGraphics 1997;17(3):707–724.
19. Shields CL, Shields JA, De Potter P. Hydroxyapatite orbital implant after enucleation: experience with initial 100 consecutive cases. Arch Ophthalmol 1992;110(3):333–338.
20. Shields CL, Shields JA, De Potter P, Singh AD. Problems with the hydroxyapatite orbital implant: experience with 250 consecutive cases. Br J Ophthalmol 1994;78(9):702–706.
21. Hunter TB, Yoshino MT, Dzioba RB, Light RA, Berger WG. Medical devices of the head, neck, and spine. RadioGraphics 2004;24(1):257–285.
22. De Potter P, Duprez T, Cosnard G. Postcontrast magnetic resonance imaging assessment of porous polyethylene orbital implant (Medpor). Ophthalmology 2000;107(9):1656–1660.
23. Su GW, Yen MT. Current trends in managing the anophthalmic socket after primary enucleation and evisceration. Ophthal Plast Reconstr Surg 2004;20(4):274–280.
24. Gale ME, Vincent ME, Sutula FC. Orbital implants and prostheses: postoperative computed tomographic appearance. AJNR Am J Neuroradiol 1985;6(3):403–407.

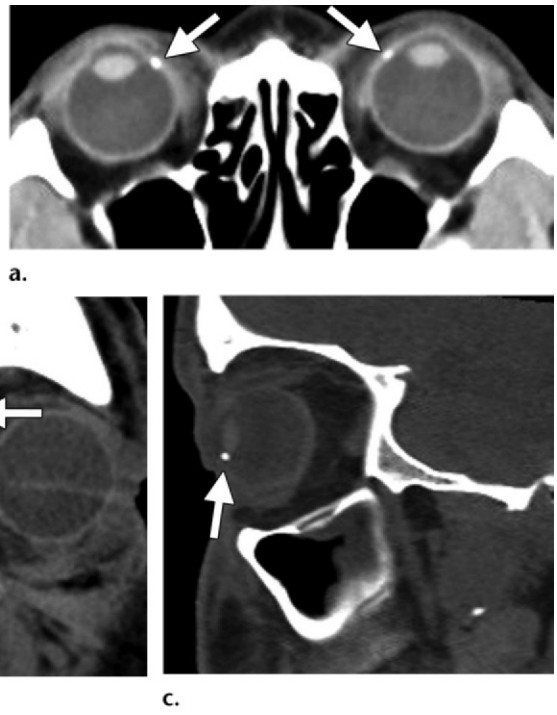

Figure 19. Potential mimics of implanted orbital devices in three patients. **(a)** Axial CT image obtained in a 79-year-old man shows calcifications at the insertion sites of the bilateral medial rectus muscles (arrows), findings pathognomonic of senescent scleral calcifications. An EX-PRESS device (cf Fig 2a) would appear higher in attenuation and be more medial in location. **(b)** Coronal CT image obtained in a 66-year-old woman shows bilateral calcifications in the region of the trochlear apparatus (arrows). **(c)** Sagittal CT image obtained in a 25-year-old man shows a punctate area of attenuation (arrow) in the anterior aspect of the globe, just below the level of the lens. An EX-PRESS device could have a similar appearance, but such devices are rarely placed in an inferior location (cf Fig 2b). Several additional metallic foci were seen in the orbit, rendering a foreign body the most likely diagnosis. On further investigation, it was discovered that the patient had sustained a gunshot wound to the face many years earlier.

25. Coskun U, Ozturk S, Zor F, Turgut AT, Sengezer M. Imaging of porous polyethylene implant by using multidetector spiral computed tomography. J Craniofac Surg 2008;19(1):156–158.
26. Lukáts O, Bujtár P, Sándor GK, Barabás J. Porous hydroxyapatite and aluminum-oxide ceramic orbital implant evaluation using CBCT scanning: a method for in vivo porous structure evaluation and monitoring. Int J Biomater 2012;2012:764749.
27. Sires BS, Holds JB, Archer CR. Postimplantation density changes in coralline hydroxyapatite orbital implants. Ophthal Plast Reconstr Surg 1998;14(5):318–322.
28. Sires BS, Holds JB, Archer CR. Variability of mineral density in coralline hydroxyapatite spheres: study by quantitative computed tomography. Ophthal Plast Reconstr Surg 1993;9(4):250–253.
29. Graue GF, Finger PT. Physiologic positron emission tomography/CT imaging of an integrated orbital implant. Ophthal Plast Reconstr Surg 2012;28(1):e4–e6.
30. Domange-Testard A, Papathanassiou D, Menéroux B, Amans J, Liehn JC. SPECT-CT images of an ocular coralline hydroxyapatite implant visible on bone scintigraphy. Clin Nucl Med 2007;32(2):132–134.
31. Flanders AE, De Potter P, Rao VM, Tom BM, Shields CL, Shields JA. MRI of orbital hydroxyapatite implants. Neuroradiology 1996;38(3):273–277.
32. Barnwell JD, Castillo M. MR imaging of progressive enhancement of a bioceramic orbital prosthesis: an indicator of fibrovascular invasion. AJNR Am J Neuroradiol 2011;32(1):E8–E9.
33. Yuh WT, Hanigan MT, Nerad JA, et al. Extrusion of eye socket magnetic implant after MR imaging: potential hazard to patient with eye prosthesis. J Magn Reson Imaging 1991;1(6):711–713.
34. Zwick OM, Seiff SR. Supportive care of facial nerve palsy with temporary external eyelid weights. Optometry 2006;77(7):340–342.
35. Seiff SR, Boerner M, Carter SR. Treatment of facial palsies with external eyelid weights. Am J Ophthalmol 1995;120(5):652–657.
36. Robey AB, Snyder MC. Reconstruction of the paralyzed face. Ear Nose Throat J 2011;90(6):267–275.
37. Schrom T, Thelen A, Asbach P, Bauknecht HC. Effect of 7.0 Tesla MRI on upper eyelid implants. Ophthal Plast Reconstr Surg 2006;22(6):480–482.
38. Marra S, Leonetti JP, Konior RJ, Raslan W. Effect of magnetic resonance imaging on implantable eyelid weights. Ann Otol Rhinol Laryngol 1995;104(6):448–452.
39. Swanger RS, Crum AV, Klett ZG, Bokhari SA. Postsurgical imaging of the globe. Semin Ultrasound CT MR 2011;32(1):57–63.
40. Ervin AM, Wojciechowski R, Schein O. Punctal occlusion for dry eye syndrome. Cochrane Database Syst Rev 2010(9):CD006775.
41. Mittelman D. Amblyopia. Pediatr Clin North Am 2003;50(1):189–196.
42. Kadom N. Pediatric strabismus imaging. Curr Opin Ophthalmol 2008;19(5):371–378.
43. Scott AB, Alexander DE, Miller JM. Bupivacaine injection of eye muscles to treat strabismus. Br J Ophthalmol 2007;91(2):146–148.
44. Scott AB, Miller JM, Shieh KR. Treating strabismus by injecting the agonist muscle with bupivacaine and the antagonist with botulinum toxin. Trans Am Ophthalmol Soc 2009;107:104–109.
45. Hart BL, Spar JA, Orrison WW Jr. Calcification of the trochlear apparatus of the orbit: CT appearance and association with diabetes and age. AJR Am J Roentgenol 1992;159(6):1291–1294.